

# Closed-loop one-way-travel-time navigation using low-grade odometry for autonomous underwater vehicles

Brian Claus  | James H. Kepper IV | Stefano Suman | James C. Kinsey

Applied Ocean Physics and Engineering, Woods Hole Oceanographic Institution, Woods Hole, MA, USA

## Correspondence

Brian Claus, Applied Ocean Physics and Engineering, Woods Hole Oceanographic Institution, Woods Hole, MA.

Email: bclaus@whoi.edu

## Abstract

This paper extends the progress of single beacon one-way-travel-time (OWTT) range measurements for constraining XY position for autonomous underwater vehicles (AUV). Traditional navigation algorithms have used OWTT measurements to constrain an inertial navigation system aided by a Doppler Velocity Log (DVL). These methodologies limit AUV applications to where DVL bottom-lock is available as well as the necessity for expensive strap-down sensors, such as the DVL. Thus, deep water, mid-water column research has mostly been left untouched, and vehicles that need expensive strap-down sensors restrict the possibility of using multiple AUVs to explore a certain area. This work presents a solution for accurate navigation and localization using a vehicle's odometry determined by its dynamic model velocity and constrained by OWTT range measurements from a topside source beacon as well as other AUVs operating in proximity. We present a comparison of two navigation algorithms: an Extended Kalman Filter (EKF) and a Particle Filter (PF). Both of these algorithms also incorporate a water velocity bias estimator that further enhances the navigation accuracy and localization. Closed-loop online field results on local waters as well as a real-time implementation of two days field trials operating in Monterey Bay, California during the Keck Institute for Space Studies oceanographic research project prove the accuracy of this methodology with a root mean square error on the order of tens of meters compared to GPS position over a distance traveled of multiple kilometers.

## KEYWORDS

acoustic, autonomous underwater vehicles, low grade odometry, navigation, one way travel time

## 1 | INTRODUCTION

Accurate absolute positioning is fundamental to all robots—both to ensure realtime closed-loop control and to provide position measurements co-located with other observations. While the global positioning system (GPS) provides meter-scale absolute positioning of terrestrial, aerial, and sea-surface robots, the rapid attenuation of GPS in water precludes its use on submerged robots. Long baseline (LBL),<sup>1</sup> ultra-short baseline (USBL)<sup>2</sup> or single transponder methods<sup>3</sup> have traditionally provided absolute positioning underwater based on ranges estimated from acoustic two-way travel times. Those methods are in contrast to strap down dead-reckoning or odometry methods such as those provided by Doppler velocity logs (DVLs) and inertial navigation systems (INSs) which accumulate error over time.<sup>4,5</sup> However, most acoustic methods extend poorly to multiple robots as only a single

submerged robot can receive and transmit acoustic positioning signals at a time. Thus, as the number of robots increases, the rate of position updates decreases proportionally to the inverse of the number of robots.

One-way-travel-time (OWTT) navigation provides a solution that enables simultaneous positioning of multiple robots from a single acoustic beacon by constraining strap-down navigation systems, and, when coupled with increasingly mature autonomous surface vessels (ASVs), provides a framework for navigating multiple submerged AUVs from one or more ASVs or in fact from an AUV which periodically surfaces.<sup>6,7</sup> Further, as will be shown in this work, the method is adaptable to low-quality odometry, avoiding the need for expensive and high-power inertial and acoustic systems. As such, the method is well suited to equipping the emerging class of low-cost micro-AUVs<sup>8,9</sup> and long-duration systems such as underwater gliders<sup>10</sup> or long-range

AUVs<sup>11</sup> with bounded error navigation. Also, it enables bounded navigation for AUV operations in the mid-water column either during descents in deep water or to provide spatially dense surveys of fine scale physical or chemical features.<sup>12</sup> It is additionally well suited to aiding navigation in under-ice studies which face the added challenge that upward facing DVLs measure the AUV speed relative to a non-inertial frame—i.e., translating and rotating ice.<sup>13</sup>

Fundamental to OWTT ranging is a synchronized time base across all platforms. Highly accurate and synchronized clocks, such as a chip-scale atomic clock (CSAC)<sup>14</sup> or a temperature compensated crystal oscillator (TXCO),<sup>15</sup> on both the beacon and the receiving vehicle are needed to accurately measure the one-way-travel-time of the acoustic packet. While CSACs initially promised an extremely stable time reference for relatively little power, recent manufacturing and aging issues have tempered those expectations.<sup>16</sup> Using this synchronized time, the time of launch and transmission location are encoded in the transmitted packet such that any receiving vehicle can compute a range from a known location with which to constrain its own navigation solution.

As the received range only constrains the navigation solution, the observability of the system is an important area of consideration, especially for single beacon ranging.<sup>17</sup> Prior efforts have proven observability of single beacon ranging through analysis of the Fisher Information Matrix<sup>18</sup> and which trajectories are observable.<sup>17</sup> Other work has examined optimal trajectories of a team of AUVs to enhance observability and thus improve the navigational accuracy.<sup>19</sup>

Other works have investigated the use of multiple cooperating vehicles which share varying amounts of information to further constrain their navigation.<sup>20–22</sup> A significant challenge in using inter-vehicle ranges for position estimates is preventing overconfidence in the solution through the sharing of correlated covariance information or double counting.<sup>23</sup> Prior work has largely dealt with this challenge by preserving prior measurement information and extending the state with each new measurement which has limited scalability and suitability for real-time processing. Approximations to this approach have been presented which compress prior measurements<sup>24</sup> or which avoid transmitting the correlation terms of the covariance matrix.<sup>25</sup>

Despite the aforementioned advantages, successful post-processing of experimental results using OWTT range measurements are rare. Salient examples include centralized<sup>15</sup> and decentralized<sup>26</sup> filters, approximate filters for bandwidth limited communications,<sup>25</sup> cooperative navigation with kayaks<sup>23</sup> and cooperative ranging and bathymetric navigation.<sup>27</sup> Rarer are results that incorporate odometry from non-DVL sources such as the recent work with underwater glider tracking over short distances<sup>21</sup> and long distances under ice.<sup>28</sup> Completely absent are presentations of experimental validations of closed-loop solutions.

This work builds upon prior efforts and presents for the first time experimental results of closed-loop OWTT navigation using multiple AUVs. Further, a direct comparison between model velocity aided odometry and DVL aided odometry is presented, illustrating the flexibility of the method. The methodology was developed based on post-processing of field data collected during the Keck Institute for Space Studies (KISS) “Satellites to the Seafloor” project conducted in Monterey Bay, CA in September, 2016.<sup>29</sup> With this data an Extended

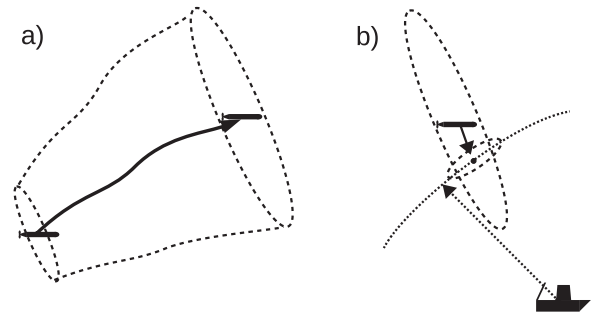


**FIGURE 1** Diagram of the one-way-travel-time navigation process where the autonomous underwater vehicle (AUV) transits in frame (a) with its estimation uncertainty growing over time. In frame (b) the AUV receives a range which reduces its uncertainty and updates its location estimate

Kalman Filter (EKF) and Particle Filter (PF) were developed each with a bias estimator. Subsequently the EKF solution was demonstrated in closed-loop feedback into the navigation solution during field trials near Woods Hole, MA.

The remainder of this paper is organized as follows: Section 2 discusses the EKF, PF and bias estimator algorithms. Section 3 describes the vehicle and experimental set-up. Section 4 presents the results from the post-processed field trials in Monterey Bay, CA and closed-loop field trials near Woods Hole, MA and Section 5 presents our conclusions.

## 2 | ONE-WAY-TRAVEL-TIME NAVIGATION WITH LOW-GRADE ODOMETRY

One-way-travel-time navigation incorporates range measurements between a transmitter and a receiver by means of acoustic packet transmissions. Based on a pre-determined timing cycle, the source transmits an acoustic packet, encoded with its pose information and time-of-launch (TOL). The receiver decodes this acoustic packet information and records its time-of-arrival (TOA). Based on the acoustic packet's time of flight (TOF), and knowledge of the transmitting medium's sound velocity profile, a range is calculated between the transmitter and the receiver. The source's position information and calculated range is then incorporated into the receiver's state estimator to update its own navigation estimate. Since the range is calculated based on TOF of the acoustic packet, both the transmitter and the receiver must have highly synchronized clocks within an acceptable tolerance. For example, a timing error of less than 1 ms will result in a position error of less than 1.5 m with a sound speed of 1500 m/s. Using this information, a range from a source beacon collapses the vehicle's position area of uncertainty and updates its position estimate as illustrated in Figure 1.

To fuse the range measurement with the vehicle's position estimate, the standard EKF for one-way-travel-time navigation is extended to include a bias estimator and to take as its navigation update a model velocity based dead-reckoning solution. We also present a particle filter implementation based on the same inputs which also includes a bias estimator.

## 2.1 | Tightly coupled OWTT extended Kalman filter

In this section, we present the EKF coupled with a bias estimator. This EKF algorithm is summarized below in Algorithm 1.

### Algorithm 1: EKF with Water Velocity Bias Estimator

- 
- 1: **Loop**
  - 2:   Process Kinematic Plant Model Prediction Step at each time step
  - 3:   **if** Receive Model-Velocity Measurement **then**
  - 4:     Process Model-Velocity measurement in EKF measurement update step
  - 5:   **else if** Receive OWTT Range measurement **then**
  - 6:     Augment State Vector & Augment Covariance Matrix with beacon position and variance
  - 7:     Linearize range equation to process range observation
  - 8:     Process range measurement in EKF measurement update step
  - 9:     Determine Water Velocity Measurement & Run Bias Estimator
  - 10:   Add velocity bias measurement to model velocity measurement
  - 11:   **end if**
  - 12: **end loop**
- 

Since we consider attitude and depth to be adequately instrumented, the three-dimensional OWTT range is projected into the horizontal plane, and only position and velocity are considered.

#### 2.1.1 | EKF process and measurement model

In this EKF, the vehicle's state vector is composed of its horizontal position and velocity components:

$$\mathbf{xv} = [x, y, u, v]^T. \quad (1)$$

Here each  $x, y$  pair is the vehicle's position, and each  $u, v$  pair the vehicle's component velocity. The vehicle's plant model is estimated by a linear Continuous White Noise Acceleration Model (i.e., a kinematic constant velocity model)<sup>30</sup> and a non-linear measurement observation model. The constant velocity model is used to make this algorithm applicable to any AUV, but it does not account for vehicle turning, thrust, and drag dynamics. As such, this model will have trouble during turns, but since most of the AUV's mission consists of long, constant velocity legs, prior work has proven that the error converges once the vehicle reaches its constant velocity state after a turn, start, or stop.<sup>31</sup>

In discrete time, the models follow the standard form

$$\mathbf{xv}_k = \mathbf{F}\mathbf{xv}_{k-1} + \mathbf{w}_{k-1} \quad (2)$$

$$\mathbf{z}_k = \mathbf{H}_k\mathbf{xv}_k + \mathbf{v}_k \quad (3)$$

where the state transition matrix  $\mathbf{F}$  maps the prior state to the present with the addition of the noise term  $\mathbf{w}$ . Here, the state transition matrix

is based on a constant velocity model with sampling period,  $dt$ :

$$\mathbf{F} = \begin{bmatrix} 1 & 0 & dt & 0 \\ 0 & 1 & 0 & dt \\ 0 & 0 & 1 & 0 \\ 0 & 0 & 0 & 1 \end{bmatrix}. \quad (4)$$

For the measurements,  $\mathbf{z}$ , the model velocity measurement along with the bias estimation is linear, and the OWTT measurement is non-linear (more details on the bias estimation are presented in Section 2.3). The plant process noise,  $\mathbf{w}_k$ , and measurement noise,  $\mathbf{v}_k$ , are considered zero-mean, Gaussian white noise:

$$\mathbf{w}_k \sim \mathcal{N}(\mathbf{0}, \mathbf{Q}) \quad (5)$$

$$\mathbf{v}_k \sim \mathcal{N}(\mathbf{0}, \mathbf{R}_k). \quad (6)$$

For the measurement variance matrix,  $\mathbf{R}$ , the matrix is diagonal with the respective measurement (i.e., GPS, model velocity, or range) variance values:

$$\mathbf{R}_{gps} = \begin{bmatrix} \sigma_{gps}^2 & 0 \\ 0 & \sigma_{gps}^2 \end{bmatrix} \quad (7)$$

$$\mathbf{R}_{vel} = \begin{bmatrix} \sigma_{vel}^2 & 0 \\ 0 & \sigma_{vel}^2 \end{bmatrix} \quad (8)$$

$$R_{rng} = [\sigma_{rng}^2]. \quad (9)$$

The plant process noise matrix,  $\mathbf{Q}$ , is defined with a gain parameter,  $\bar{q}$ :

$$\mathbf{Q} = E[\mathbf{v}(k)\mathbf{v}(k)^T] = \begin{bmatrix} \sigma_x^2 & 0 & 0 & 0 \\ 0 & \sigma_y^2 & 0 & 0 \\ 0 & 0 & \sigma_u^2 & 0 \\ 0 & 0 & 0 & \sigma_v^2 \end{bmatrix} \bar{q}. \quad (10)$$

Assuming that the state estimation of position and velocity are independent, cross terms may be neglected and the  $\mathbf{Q}$  matrix becomes a diagonal matrix.

The EKF updates the state estimate at each time step,  $k$ , with a prediction step and subsequent measurement update depending on availability of a measurement.<sup>32</sup>

The state is predicted by applying the transition matrix,  $\mathbf{F}$ , to the state estimate of the previous step:

$$\hat{\mathbf{x}}_k^- = \mathbf{F}\hat{\mathbf{x}}_{k-1}^+ \quad (11)$$

Subsequently, the predicted error covariance matrix,  $\mathbf{P}^-$ , is determined by applying the plant transition matrix to the updated error covariance matrix of the previous step,  $\mathbf{P}^+$  and the process noise covariance matrix,  $\mathbf{Q}$ :

$$\mathbf{P}_k^- = \mathbf{F}\mathbf{P}_{k-1}^+ \mathbf{F}^T + \mathbf{Q}. \quad (12)$$

With the availability of a measurement, the Kalman Gain matrix,  $\mathbf{K}$ , is computed by being a function of the predicted error covariance, the respective measurement mapping matrix  $\mathbf{H}$ , and the respective measurement noise covariance matrix  $\mathbf{R}$ :

$$\mathbf{K}_k = \mathbf{P}_k^- \mathbf{H}_k^T (\mathbf{R}_k + \mathbf{H}_k \mathbf{P}_k^- \mathbf{H}_k^T)^{-1}. \quad (13)$$

The state estimate is then updated by adding the product of the Kalman Gain and the measurement innovation to the predicted state:

$$\hat{\mathbf{x}}_k^+ = \hat{\mathbf{x}}_k^- + \mathbf{K}_k (\mathbf{z}_k - \mathbf{H}_k \hat{\mathbf{x}}_k^-). \quad (14)$$

Lastly, the error covariance is updated using the "Joseph form" of the Riccati equation, which ensures positive definiteness:<sup>33</sup>

$$\mathbf{P}_k^+ = (\mathbf{I} - \mathbf{K}_k \mathbf{H}_k) \mathbf{P}_k^- (\mathbf{I} - \mathbf{K}_k \mathbf{H}_k)^T + \mathbf{K}_k \mathbf{R} \mathbf{K}_k^T. \quad (15)$$

### 2.1.2 | Range measurement and augmentation

For each OWTT range measurement, from either the surface beacon or another vehicle, the receiving vehicle's state vector and error covariance matrix,  $\mathbf{P}$ , is augmented to process the range measurement with the transmitting beacon's pose,  $x_b, y_b$ :

$$\mathbf{x}_{aug} = [x, y, u, v, x_b, y_b]^T. \quad (16)$$

The covariance matrix is augmented with the transmitting beacon's position uncertainty values, similar to the Naively Distributed Extended Kalman Filter (NEKF).<sup>34</sup> There, the authors show that a geometry that consists of a single surface transmitting node with multiple submerged transmitting nodes (which mirrors the geometry in our field experiments), the NEKF closely follows the  $1\sigma$  uncertainties of the benchmark Centralized EKF. A similar arrangement has also been termed the Egocentric Extended Kalman Filter (EEKF) which assumes independence among the vehicles ranging by neglecting the cross covariance terms.<sup>25</sup> Motivated by these prior results, the algorithmic simplicity, and low acoustic bandwidth necessary, we use a similar method during the transmitting of beacon state uncertainties. Here, the vehicles covariance  $\mathbf{P}_v$  is augmented with the beacon's covariance  $\mathbf{P}_b$  to form the augmented covariance matrix  $\mathbf{P}_{aug}$  to process the range measurement:

$$\mathbf{P}_{aug} = \begin{bmatrix} \mathbf{P}_v & \mathbf{0} \\ \mathbf{0} & \mathbf{P}_b \end{bmatrix}. \quad (17)$$

The  $\mathbf{P}_v$  matrix is the vehicle's predicted  $4 \times 4$  Covariance Matrix,  $\mathbf{P}^-$ , at time,  $k$ , of the range measurement. The  $\mathbf{P}_b$  matrix is a  $2 \times 2$  diagonal matrix, in which the diagonals are both equal to the sum of the beacon's variance values requiring only a single value to be transmitted in the acoustic packet. Transmitting beacon uncertainties in this manner is more conservative than the NEKF or EEKF methods and thus minimizes the potential for overconfident solutions.

Once this augmentation process is complete, the measurement matrix,  $\mathbf{H}_{rng}$  is determined to map the vehicle's state vector to the OWTT range computed by the product of the acoustic packet's TOF and sound speed. The OWTT range update is based upon the decentralized EKF presented prior.<sup>35</sup> Here,  $\mathbf{x}_b$  is the state vector of the beacon (either a surface beacon with access to GPS or another submerged AUV):

$$\mathbf{x}_b = [x, y]^T. \quad (18)$$

The range between the vehicle at TOA and the beacon at TOL is found by computing the linear distance between their locations:

$$zrng = \sqrt{(\mathbf{x}_{v_{xy}} - \mathbf{x}_{b_{xy}})^T (\mathbf{x}_{v_{xy}} - \mathbf{x}_{b_{xy}})} + v_{rng}. \quad (19)$$

Here,  $\mathbf{x}_{v_{xy}}$  and  $\mathbf{x}_{b_{xy}}$  are the position of the vehicle at TOA and beacon at TOL, respectively, and  $v_{rng}$  is the noise in the range measurement that does not change with time. The range equation may then be rewritten in state vector form

$$zrng = (\mathbf{x}^T \mathbf{M}^T \mathbf{M} \mathbf{x})^{1/2} + v_{rng} \quad (20)$$

where

$$\mathbf{M} = [\mathbf{J}_v \quad -\mathbf{J}_b], \quad v_{rng} \sim \mathcal{N}(\mathbf{0}, \mathbf{R}_{rng}). \quad (21)$$

Here,  $\mathbf{J}_v$  and  $\mathbf{J}_b$  are matrices defined to capture the pose information of the vehicle and the beacon at TOA and TOL, respectively.\* Since the range measurement is non-linear, a Jacobian matrix, evaluated at the vehicle's augmented predicted state becomes

$$\begin{aligned} Hrngk &= \left. \frac{\partial zrng}{\partial \mathbf{x}} \right|_{\mathbf{x}=\hat{\mathbf{x}}_{aug}^- k} \\ &= [(\hat{\mathbf{x}}_{aug}^- k)^T (\mathbf{M}^T) (\mathbf{M}) (\hat{\mathbf{x}}_{aug}^- k)]^{-1/2} (\hat{\mathbf{x}}_{aug}^- k)^T (\mathbf{M}^T) (\mathbf{M}). \end{aligned} \quad (22)$$

The Kalman Filter measurement update equations (13–15) are then processed to update the vehicle's pose with the new range measurement. The elements in the augmented state vector and augmented  $\mathbf{P}$  matrix corresponding to the receiving vehicle's state variables are then saved and are processed in the Kalman Filter prediction equations (11–12) for the next time step.

## 2.2 | Loosely coupled OWTT particle filter

In this section, we present a particle filter (PF) which provides an update to the EKF based on the OWTT ranging. The PF is presented to provide a comparative method which better captures the non-linearities in the range measurement update. Here, the PF also includes a bias estimator and takes the place of EKF's range measurement augmentation and bias estimator presented in Section 2.3. The PF algorithm is presented in Algorithm 2.

\*  $\mathbf{J}_v = [\mathbf{I}_{2 \times 2} \quad \mathbf{0}_{2 \times 2}]$ ,  $\mathbf{J}_b = \mathbf{I}_{2 \times 2}$

## Algorithm 2: PF with Water Velocity Bias Estimator

---

```

1: Loop
2:   Process Kinematic Plant Model Prediction Step at each time
   step
3:   if Receive Model-Velocity Measurement then
4:     Process measurement in EKF measurement update step
5:   else if Receive OWTT Range measurement then
6:     for  $i = 1$  to  $N$  do
7:       Propagate particle by DR and apply jitter
8:       Compute weight
9:     end for
10:    Normalize weights
11:    Re-sample
12:    Compute state estimate
13:    Compute water velocity bias
14:  end if
15: end loop

```

---

In the PF algorithm, the EKF's dead-reckoning solution since the last range update is used to propagate the prior particles  $\mathbf{x}_{k-1}^i$  with the state difference  $\Delta \mathbf{x}_k$ . To account for the error growth in the dead-reckoning solution, a proportionate amount of jitter  $\mathbf{r}_k$  is applied during the particle propagation proportional to the distance traveled through the  $\alpha_{DR}$  term:

$$\mathbf{x}_k^i = \mathbf{x}_{k-1}^i + \Delta \mathbf{x}_k + \mathbf{r}_k \quad (23)$$

$$\mathbf{r}_k = \mathcal{N}(0, \alpha_{DR} \|\Delta \mathbf{x}_k\|). \quad (24)$$

Here, the range time step is indicated by  $k$ , the number of particles by  $N$  and the particle index by  $i$ . The particle weights  $\tilde{w}_k^i$  are then computed by comparing the range measurement  $z_k$  with the estimated range from each particle to the transmitting beacon's location  $\mathbf{x}_b$  using a normal distribution:

$$\tilde{w}_k^i = p(z_k \| \|\mathbf{x}_k^i - \mathbf{x}_b\|, \sigma_{pf}). \quad (25)$$

The normal distribution is defined by  $\sigma_{pf}$ , estimated using a range dependent error term  $\alpha_{rng}$  and the square root of the norm of the beacon's position estimate co-variance  $\mathbf{P}_b$ :

$$\sigma_{pf} = \alpha_{rng} * z_k + \|\mathbf{P}_b\|^{1/2}. \quad (26)$$

The raw particle weights  $\tilde{w}_k^i$  are then normalized to  $w_k^i$  such that their sum is equal to one to form them into a probability distribution:

$$w_k^i = \frac{\tilde{w}_k^i}{\sum_{i=1}^N \tilde{w}_k^i}. \quad (27)$$

To adjust the particle locations so they best capture the informative portion of the probability density function the particles are then re-sampled. While there are several options for re-sampling algorithms here we use systematic re-sampling outlined in Algorithm 3.<sup>36</sup> This

method provides a fast and simple way to represent the probability density through evenly weighted particles, requiring the particle locations and weights as inputs and providing the re-sampled particles as outputs. The algorithm operates by first taking the cumulative sum of the particle weights, forming an increasing set of values from zero to one. A random number is then drawn from a uniform distribution on the interval  $[0,1]$  and the index of the cumulative sum found in which the random number is equal to the value of the cumulative sum. The particle at the index in the old set is then stored at  $i$  in the re-sampled set for output. In this way, particles with high weight are divided into many particles as they occupy a large portion of the cumulative sum and particles with small weights are discarded as they occupy a negligible portion of the cumulative sum.

## Algorithm 3: Systematic Re-Sampling

---

```

1: Cumulative sum of weights
2: for  $i = 0$  to  $N$  do
3:   Draw random number on  $[0,1]$ 
4:   Find index of random number in cumulative sum
5:   Store particle at index for output
6: end for

```

---

The updated state  $\hat{\mathbf{x}}_k$  may then be estimated by simply computing the average of the re-sampled particles locations:

$$\hat{\mathbf{x}}_k = \frac{1}{N} \sum_{i=1}^N \mathbf{x}_k^i. \quad (28)$$

The updated state estimate is then fused back into the EKF's navigation solution which continues dead-reckoning on every speed estimate until the next range is received.

## 2.3 | Velocity bias estimator

For dead-reckoning AUVs moving in mostly straight lines the primary source of error accumulation may be assumed to be due to unknown and varying ocean currents and modeled velocity estimation errors. These errors present themselves as a persistent bias in the state update if they are changing much slower than the frequency of range measurements. To improve the dead-reckoning performance a velocity bias estimator may be written based on the state update bias and the time difference between ranges. With each range measurement, the EKF or PF output may be used to determine a velocity error measurement:

$$\mathbf{z}_{vel} = \frac{(\hat{\mathbf{x}}_{x,y}^+ - \hat{\mathbf{x}}_{x,y}^-)_{TOA}}{\Delta t}. \quad (29)$$

Here,  $\Delta t$  is the time between the current range measurement and the previous range measurement, and  $x, y$  refer to the position variables of the vehicle's state. Further, a clock bias estimator may be included based on the difference between the range measurement and the range estimate from the difference of the EKF's or PF's state estimate and the beacon location. To estimate these biases the EKF and PF are extended with a Kalman Filter (KF) whose state includes the XY velocity and clock bias. This process of separating the bias estimation from the primary estimator breaks off the linear portion of the estimator from the non-linear portion, keeping the number of states in the non-linear portion small.<sup>37</sup>

$$\mathbf{x}_{bias} = \begin{bmatrix} \bar{v}_x \\ \bar{v}_y \\ \bar{t} \end{bmatrix}. \quad (30)$$

With the  $\bar{\mathbf{F}}$  and  $\bar{\mathbf{H}}$  matrices equal to the identity matrices, the KF predicts the bias estimator co-variance  $\bar{\mathbf{P}}^-$  through addition of the prior bias estimator covariance and the process noise covariance matrix  $\bar{\mathbf{Q}}$ :

$$\bar{\mathbf{P}}_k^- = \bar{\mathbf{F}}\bar{\mathbf{P}}_{k-1}^+ \bar{\mathbf{F}} + \bar{\mathbf{Q}}. \quad (31)$$

The bias estimator covariance prediction is then used to compute the co-variance innovation  $\bar{\mathbf{S}}$  through addition of the EKF or PF covariance  $\mathbf{P}^+$  for the velocity bias and the norm of the EKF or PF covariance for the time bias:

$$\bar{\mathbf{S}}_k = \bar{\mathbf{P}}_k^- + \begin{bmatrix} \mathbf{P}_k^+ & \mathbf{0} \\ \mathbf{0} & ||\mathbf{P}_k^+|| \end{bmatrix}. \quad (32)$$

The measurement innovation  $\bar{\mathbf{y}}$  is computed through the subtraction of the bias estimator state prediction from the velocity measurement in Eq. (29) and the quotient of the range error estimate and the sound speed:

$$\bar{\mathbf{y}}_k = \begin{bmatrix} zvel, k \\ (z_{rng, k} - ||\hat{\mathbf{x}}_{xy, k}^- - \mathbf{x}_b||)v_{ss}^{-1} \end{bmatrix} - \bar{\mathbf{H}}\hat{\mathbf{x}}_{bias, k-1}. \quad (33)$$

The Kalman gain  $\bar{\mathbf{K}}$  is then computed as the product of the predicted covariance and inverted covariance innovation.

$$\bar{\mathbf{K}}_k = \bar{\mathbf{P}}_k^- \bar{\mathbf{H}} \bar{\mathbf{S}}_k^{-1} \quad (34)$$

Using these terms, the bias estimator's state and covariance are updated through application of the Kalman gain to the measurement innovation and by the sequential algebraic Riccati equation respectively:

$$\hat{\mathbf{x}}_{bias, k} = \hat{\mathbf{x}}_{bias, k-1} + \bar{\mathbf{K}}_k \bar{\mathbf{y}}_k \quad (35)$$

$$\bar{\mathbf{P}}_k^+ = \bar{\mathbf{P}}_k^- + \bar{\mathbf{K}}_k \bar{\mathbf{S}}_k \bar{\mathbf{K}}_k^T. \quad (36)$$

The outputs of this KF are used to adjust the velocity estimates in the EKF and to adjust the received range estimates. Previous work has described a similar method to the one described here that estimates range-based averaged currents (RACs) for use with underwater gliders.<sup>28</sup> That approach estimates a new current estimate after a series of OWTT range measurements. Conversely, the bias estimator in this work conducts a new estimate sequentially after each OWTT measurement from any beacon.

### 3 | EXPERIMENTAL CONFIGURATION

The vehicles used during all of the field trials were Ocean-Server, Inc. Iver-2 AUVs. Two of these vehicles, Iver-106 and Iver-107, were Ecomapper variants equipped with a Woods Hole Oceanographic Institution (WHOI) 25-kHz acoustic micro-modem,<sup>38</sup> a SonTek Doppler velocity log (DVL), an Ocean-Server compass for attitude estimation, and a depth sensor. The third Iver-2 vehicle, Iver-136, was similarly equipped with the WHOI micro-modem 2, compass and depth sensor. Additionally, that vehicle has a dual upward, downward facing 600 kHz RDI phased array DVL, a Microstrain 3DM-GX3-25 and an APS-1540 fluxgate magnetometer. These vehicles, along with the key components used in this work, are shown on board the R/V *Shana Rae* in Figure 2.

All three Iver-2 AUVs software systems were modified to use 14.04 Ubuntu Linux with the existing control computer running on the Linux stack in a virtual machine. In this manner the Deep Submergence Laboratory's library of software built around the Lightweight Communication and Marshaling (LCM) protocol could be leveraged and built upon.<sup>39</sup> Specifically a C++ framework for the implementation of real-time Kalman Filters and Extended Kalman Filters was developed and used. In this framework, a base class has methods to execute the computations that are common to all Extended Kalman Filters through an interface to high-performance linear algebra libraries, whereas a derived class that inherits from this base class provides methods to set the elements of the matrices that are application-specific and that could be time-varying. This approach enabled an effective validation of the filter common components in the base class, while exposing a clear and easy to use interface for the implementation of the filter relevant to this application. The application-specific filter developed using this framework was integrated in NavEst, the Deep Submergence Laboratory's navigation software. NavEst used LCM to interface with multiple sensor drivers running in separate processes, enabling effective simulation and data replay capabilities of the real-time navigation core engine.

For timing, a PPSBoard, as discussed previously,<sup>40,41</sup> that incorporates a SeaScan Inc. temperature-compensated crystalline oscillator was integrated for use as a precision reference. The PPSBoard is linked to the vehicle's pulse per second (PPS) signal output from the GPS receiver. It also receives the GPS's NMEA strings and synchronizes its PPS signal to the GPS derived PPS whenever a valid string is parsed. The PPS signal from the PPSBoard is transmitted to the linux stack on the Carrier Detect pin on a RS232 port. The PPSBoard also sends an NMEA string to the linux stack which enumerates the PPS signal.



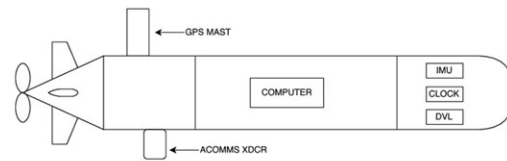
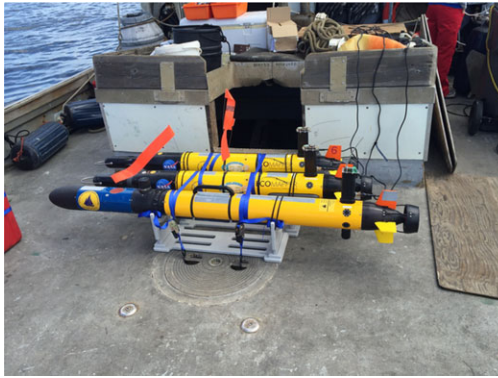


**FIGURE 2** AUVs used in the research field trials where from front to back the vehicles are the Iver-136, Iver-107, Iver-106 (left). Layout of key AUV systems used in this work (right)

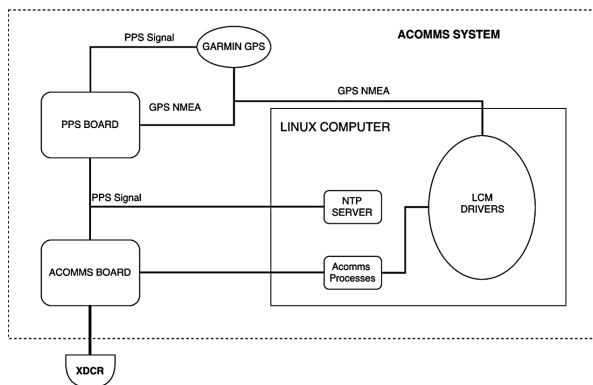


**FIGURE 3** Block Diagram for the Acoustic Communications system for both the topside and vehicle nodes

These signals are received by an ATOM Network Time Protocol (NTP) Server which runs on board each vehicle, enabling precision timekeeping by the kernel. The PPS signal from the PPSBoard also feeds into the WHOI micro-modem2 enabling the modem to precisely time transmit and receive events. Since the RS232 ports in the Iver-2 vehicles do not have CD lines, a USB-serial converter was used. As such, the polling frequency of the USB bus of 1 kHz limits the timing accuracy of the kernel to about 0.5 ms. In practice, the NTP servers on each of vehicles were not observed to drift relative to each beyond the error due to the polling frequency as the vehicles had regular access to GPS for synchronization. Thus, for a nominal sound speed velocity of 1500 m/s the timing induced error is below 1 m.

In this work the topside acoustic transducer was dangled from the support vessel. The topside's timing configuration was the same as the AUVs except a stand-alone Garmin GPS-16HVS was used and the software was running on a laptop aboard the support vessel. A general schematic of the acoustic communications topology is shown in Figure 3.

The vehicles and the topside transmitted on a fixed time division multiple access (TDMA) cycle with a period of 60 s. In the cycle each vehicle was allocated 10 s to allow sufficient time to reach all vehicles with some buffer for clearing of the acoustic channel. The top of the minute reset of the TDMA cycle and 10 s vehicle interval facilitated easy interpretation by human operators. The remaining 20 s in

the cycle was left for user initiated commands from the topside to the vehicles such as two-way range, stop mission, start mission and change way-point.

The dead-reckoning algorithm in this work uses an estimated velocity computed from the commanded propeller speed. This model was established by driving the vehicles at the surface of a lake at different commanded propeller speeds and measuring the speed given by the GPS. The submerged speed will be slightly different due to additional drag while the vehicle is at the surface. To compensate for this difference, the surface speed model is adjusted by performing shallow dives in straight lines in the lake. Afterwards, the speed model is adjusted for these dives such that the surfacing error between the last dead-reckoned location and first good GPS location is minimized.

## 4 | FIELD TRIALS

Two sets of field trials were used to perform this work. The first set of trials took place in the Monterey Bay Canyon as part of the Keck Institute for Space Studies funded "Satellites to the Seafloor" year one research project from August 27, 2016 to September 5, 2016. These trials were used to develop the algorithms based on the logged data. Subsequently, a further set of trials were performed in October 2016 in Ashumet Pond near Woods Hole, MA to examine the closed-loop performance of the OWTT multi-vehicle navigational aiding.

### 4.1 | Monterey bay field trials

In these trials the Iver-2 AUVs were deployed from the R/V *Shana Rae* based out of Santa Cruz, CA, to locations determined to be interesting based on a 300 m gridded regional ocean model. The field trial data presented in the next section is from data gathered during deployments on September 1 and 2, 2016 with locations shown in Figure 4. For the data gathered on September 1, Iver-106 and Iver-107 were in the water performing the top and bottom half of a 3 km butterfly pattern. Because of logistical problems the data from Iver-107 was not logged, however, Iver-106 was still able to benefit from its acoustic transmissions. On September 2, Iver-106 and Iver-107 were deployed to perform a complete 3km butterfly pattern but in opposite directions. On each day the topside transducer was dangled from the R/V *Shana*

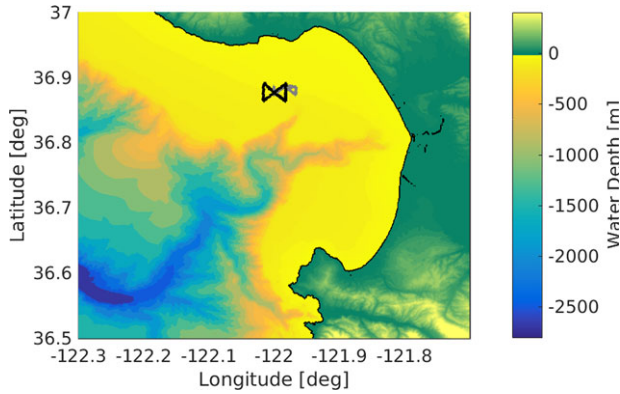


**FIGURE 4** Location of field trials in Monterey Bay California showing the tracklines of the AUVs for the Sept. 1 (gray) and Sept. 2 trials (black)

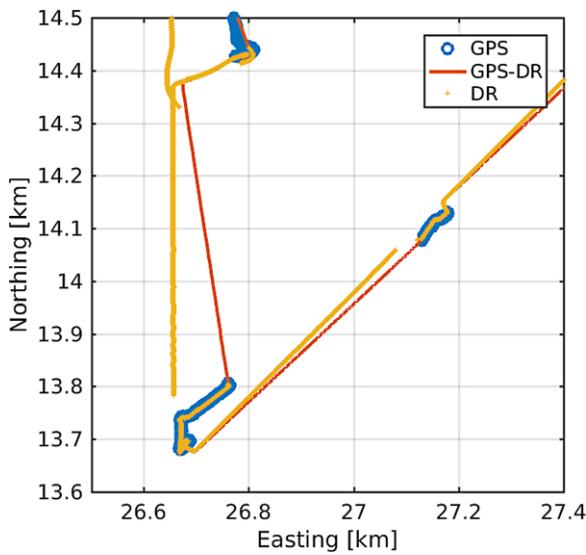


**FIGURE 5** Locations of the GPS fixes and dead-reckoning (DR) showing the GPS corrected dead-reckoning (GPS-DR) which takes the difference between the last dead-reckoned location and the first GPS location upon surfacing to compute a depth averaged water velocity over the prior segment. The depth average water velocity is then used to correct the DR to the GPS-DR

*Rae* which drifted in a central position, re-positioning as needed to maintain communications with the submerged vehicles. For all of these deployments the AUVs were programmed to perform repeated profiles (yos) down to 10 m altitude or 80 m depth. The AUVs used model velocity based dead-reckoning to navigate between waypoints spaced evenly along each length of the butterfly pattern.

Because of the use of dead-reckoning the AUVs navigation error grows between surfacing due to the ocean currents in the region which are not accounted for and to errors in the heading reference. To provide a comparative location for the navigation results developed here the dead-reckoned solution is corrected in post-processing with a water velocity estimate based on the difference between the last dead-reckoned location and first GPS location upon surfacing as illustrated in Figure 5.

**TABLE 1** Parameters used in the EKF

Parameter	Value
$\sigma_{vel}$	1 (m/s)
$\sigma_{GPS}$	10 (m)
$\sigma_{rng}$	$0.015 z_k$ (m)
$\sigma_{bias}$	0.25 (m/s)

**TABLE 2** Parameters used in the PF

Parameter	Value
$N$	2000
$\alpha_{DR}$	0.4
$\alpha_{rng}$	$0.015 z_k$ (m)

In this estimate, the water velocities are assumed to be constant over the prior segment and their effects averaged over the water column. The GPS corrected dead-reckoning was then used as a benchmark for the development of the EKF and PF solution. Using this data the parameters for the EKF and the PF were selected to minimize the error across all of the field deployments.

Specifically, for the EKF implementation,  $Q$  is set to the identity matrix  $I$

$$Q = I \quad (37)$$

and the velocity, GPS, range and bias estimate standard deviations as in Table 1. For the PF implementation the number of particles  $N$ , the dead-reckoning error growth rate  $\alpha_{DR}$ , and the range dependent error  $\alpha_{rng}$  are shown in Table 2.

For the bias estimator terms we use a value of one, for the velocity bias terms and for the clock bias term we use a value of 0.0001:

$$Q = \begin{bmatrix} 1 & 0 & 0 \\ 0 & 1 & 0 \\ 0 & 0 & 0.0001 \end{bmatrix}. \quad (38)$$

Several different scenarios may be considered in post-processing the data to examine the utility of each method. The first scenario considered is that of simply re-navigating the raw data where the vehicles come to the surface periodically, use GPS to correct any accrued error and submerge again. Here we also use the bias estimation and accept transmissions from all vehicles. The second scenario is that of only using the GPS for initializing the navigation solution and dead-reckoning from that point on-wards while still using the bias estimation and all beacons transmissions. To examine the utility of the bias estimator, the third scenario does not use the bias estimator or GPS once initialized but does use transmissions from all the beacons. The last scenario only uses transmissions from the topside beacon, uses the bias estimator but not GPS after initialization. The performance of the EKF and the PF in the second scenario, where GPS is only used for initialization, is illustrated in Figure 6 for the data from Iver-106 and Iver107 on September 2, 2017.

During these trials, both vehicles were deployed in the upper left hand corners of Figure 6 from the R/V *Shana Rae*. Iver-106 performed



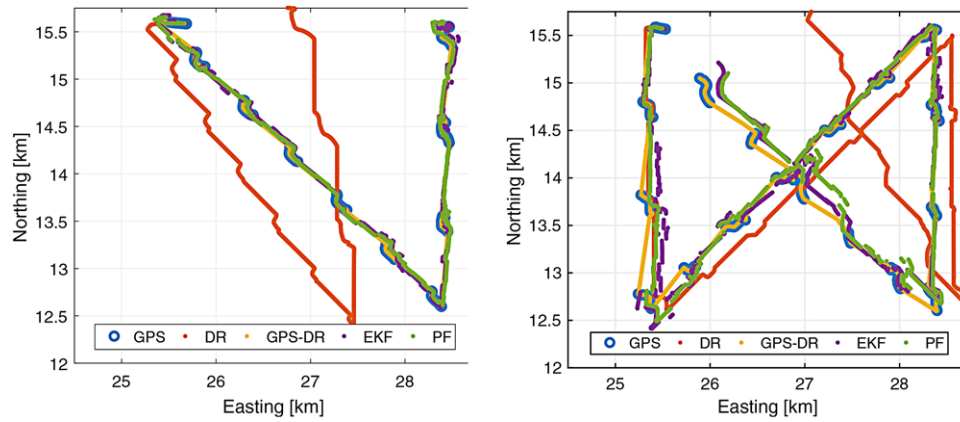


**FIGURE 6** Performance of the one-way-travel-time EKF and PF with bias estimation where the GPS is only used for initialization for Iver-106 (left) and Iver-107 (right) during the September 2 field trials in Monterey Bay, CA

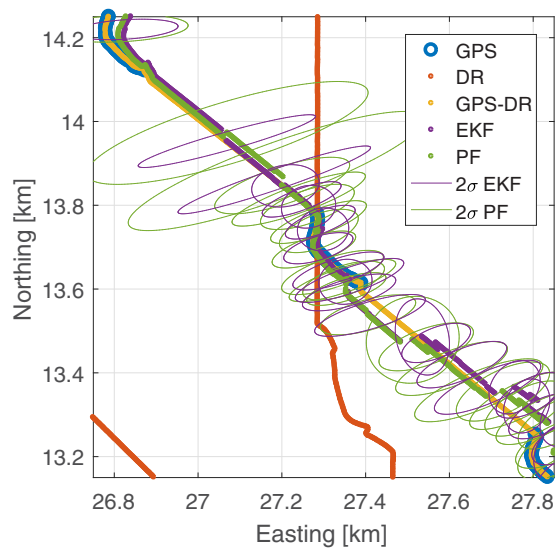


**FIGURE 7** Close up of Iver-106 during the September 2 field trials in Monterey Bay, CA where the vehicle is traversing from top left to bottom right. Both the EKF and the PF show similar performance. The top left shows a period of sparse range measurements after which the  $2\sigma$  error ellipses are initially large but converge after several successful ranges. The bias estimator also shows its utility to provide a decent estimate of the velocity bias during the gap in range updates as the EKF and PF trajectories track the GPS-DR well

the first two legs before having its propeller fouled with seaweed, necessitating its recovery. The other vehicle, Iver-107, was able to perform all four legs of its mission, requiring recovery due to its batteries being depleted. In re-navigating this data both the EKF and the PF are able to maintain convergence with errors dependent on the inter-vehicle geometry and success rate of receptions. The similarity between the two algorithms, their ability to handle gaps in received ranges and the ability of the bias estimator to improve the solution is illustrated in Figure 7.

The RMS error from each vehicle during this scenario is shown against the  $2\sigma$  bounds in Figure 8. Here the gap in ranges for Iver-106 from Figure 7 is seen around the 2500 s mark in the top frame. Additionally, after around 8300 s, Iver-106 is recovered. During this process

**TABLE 3** RMS Errors for the EKF and PF during the sept 1 and 2 experiments for vehicle's Iver-106 and Iver-107 which both use the GPS readings during surfacings (All) or ignore GPS readings except during initialization (Init), make use of the bias estimation (Yes/No) and make use all available beacons (All) or only the topside beacon (Top)

Date	Vehicle	GPS	Bias	Beacons	EKFe	PFe	DRe
Sept1	106	All	Yes	All	23 m	17 m	24 m
Sept1	106	Init	Yes	All	67 m	61 m	1500 m
Sept1	106	Init	No	All	91 m	93 m	1500 m
Sept1	106	Init	Yes	Top	212 m	119 m	1500 m
Sept2	106	All	Yes	All	17 m	8 m	16 m
Sept2	106	Init	Yes	All	41 m	31 m	855 m
Sept2	106	Init	No	All	44 m	48 m	855 m
Sept2	106	Init	Yes	Top	139 m	180 m	855 m
Sept2	107	All	Yes	All	29 m	18 m	24 m
Sept2	107	Init	Yes	All	92 m	94 m	444 m
Sept2	107	Init	No	All	205 m	93 m	444 m
Sept2	107	Init	Yes	Top	91 m	146 m	444 m

the topside transducer was pulled up on the R/V *Shana Rae* to allow for transiting to the recovery location. The effects of this process on Iver-107's navigation solution are seen from the 8300 s to just past the 10000 s mark. At this point both Iver-106 and the topside transducer were on deck. The topside transducer was subsequently put back into the water around the 11000 s mark after which the navigation solution re-converged. However, due to the lack of the other vehicle the errors and error bounds are larger past this point.

The summary of all of the different scenarios are listed in Table 3. In general, the PF implementation seems to slightly out-perform the EKF solution. In every case the PF improves on the DR error whereas the EKF improves on the error in every case except when the GPS is used throughout. During these missions the vehicle's submerged segments are only about 10 to 12 min long over a distance of around 600 to 800 m. When the GPS is used as available there is very little difference among the PF, EKF and the DR solutions as the errors accrued over this time are also small. However, when the GPS is only used for

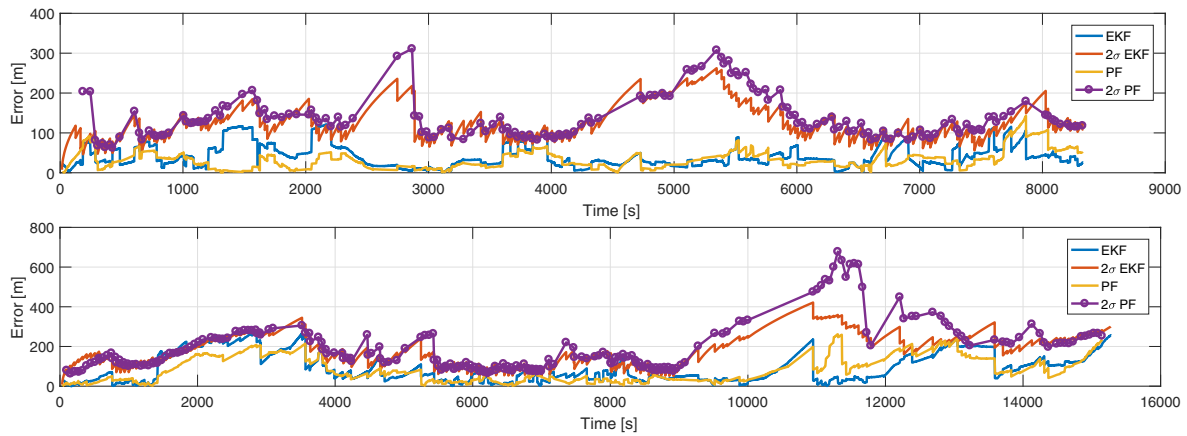


**FIGURE 8** Errors and  $2\sigma$  error bounds of Iver-106 (top) and Iver-107 (bottom) during the September 2 field trials in Monterey Bay, CA. Here, Iver-106 is recovered after 8300 s and the topside transducer is recovered from 9000 to 11000 s to facilitate recovery of Iver-106

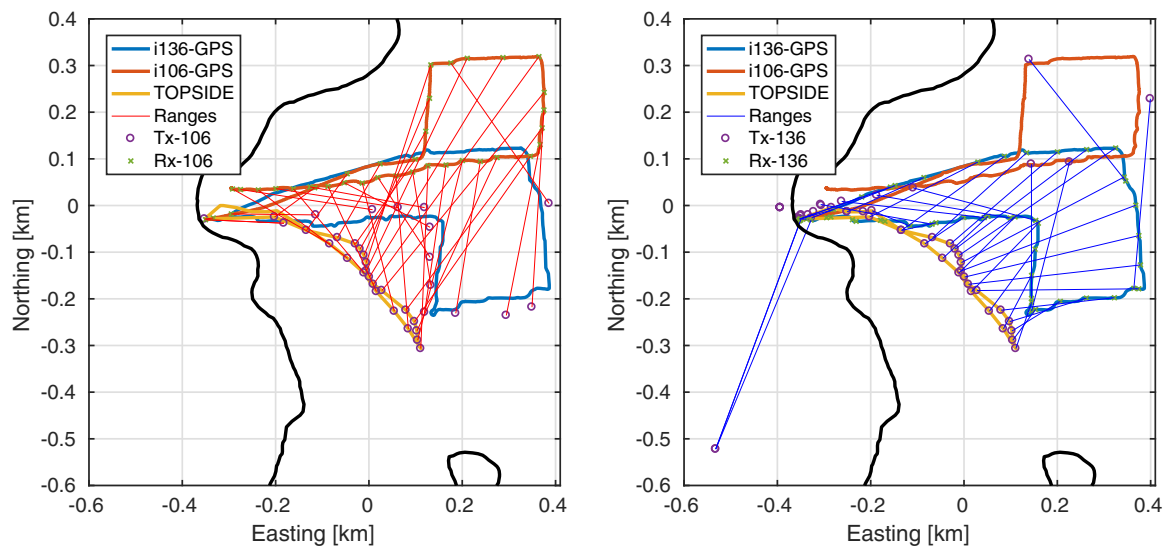


**FIGURE 9** Overview of vehicle tracks for Iver-136, Iver-106 and the R/V *Aurelia* (topside) for the October 25, 2016 closed-loop trials in Ashumet Pond. Ranges are shown between the estimated transmission location and the GPS location of the receiving vehicle for Iver-106 (Left) and Iver-136 (Right)

initializing the DR solution the differences become more pronounced. For instance, when the bias estimator and all received beacons used, the DR errors of 1500 m, 855 m and 444 m are reduced to 67 m 41 m, and 92 m for the EKF and 61 m, 31 m and 93 m for the PF during the September 1, Iver-106, September 2, Iver-106 and September 2, Iver-107 field trials respectively. If the bias estimation is not used the error increases slightly in most cases and when only the topside beacon is used the error generally increases further. These use cases illustrate the effectiveness of using multiple sources to constrain the error and the importance of bias estimation to capture persistent errors in the velocity and time estimates of each platform.

## 4.2 | Ashumet pond field trials

Subsequent to the Monterey Bay Field Trials, closed-loop multi-vehicle one-way-travel-time navigation was performed during field trials in Ashumet Pond on October 25, 2016. In these trials Iver-106 and Iver-136 were run on the surface such that the GPS measurements could

be used as ground truth while not being integrated into the navigation solution except for initialization. The topside was dangled from the R/V *Aurelia*, a small rigid hull inflatable boat. Additionally, Iver-106 was allowed to have its DVL measurements integrated into the navigation solution while Iver-136 used the model velocity estimates based on the propeller speed. This difference allows for a direct comparison between closed-loop multi-vehicle one-way-travel-time navigation that uses DVL or model velocity based dead-reckoning for its measurement update. The GPS tracks for each vehicle and the R/V *Aurelia* are shown in Figure 9 along with the successful ranges drawn from the transmission location estimate to the vehicle's GPS location.

A summary of the trajectories of Iver-106 and Iver-136 during these field trials are shown in Figure 10, the errors during the closed-loop results in Figure 11 and a summary of the RMS errors in Table 4.

During these trials the vehicles were deployed from shore. Iver-136 was prepared and deployed first, followed by Iver-106 once

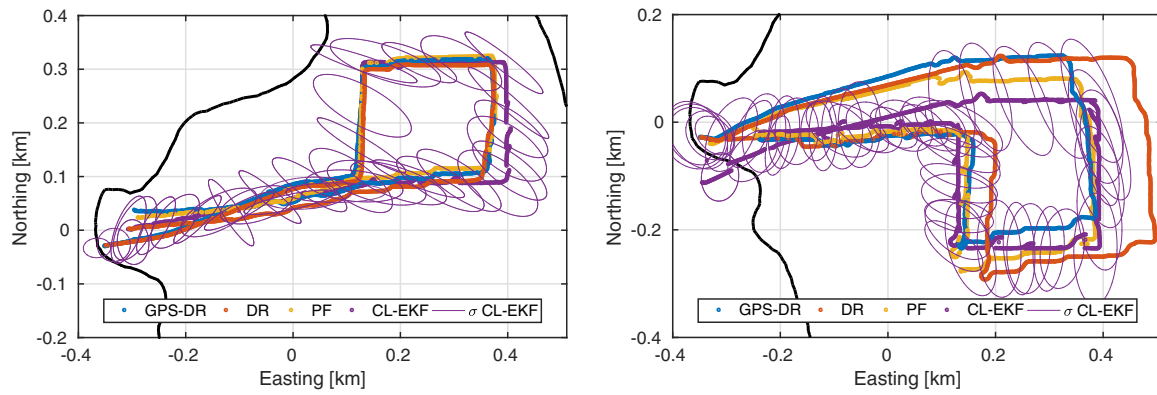


**FIGURE 10** Trajectories of the closed-loop one-way-travel-time trials for Iver-106 (Left) and Iver-136 (Right) during the October 25, 2016 field trials in Ashumet Pond. During these trials Iver-106 used the DVL in its navigation solution while Iver-136 used model velocity based dead-reckoning. The on-line closed-loop EKF solution with its  $\sigma$  error bounds are shown against the GPS corrected dead-reckoning and off-line PF solution

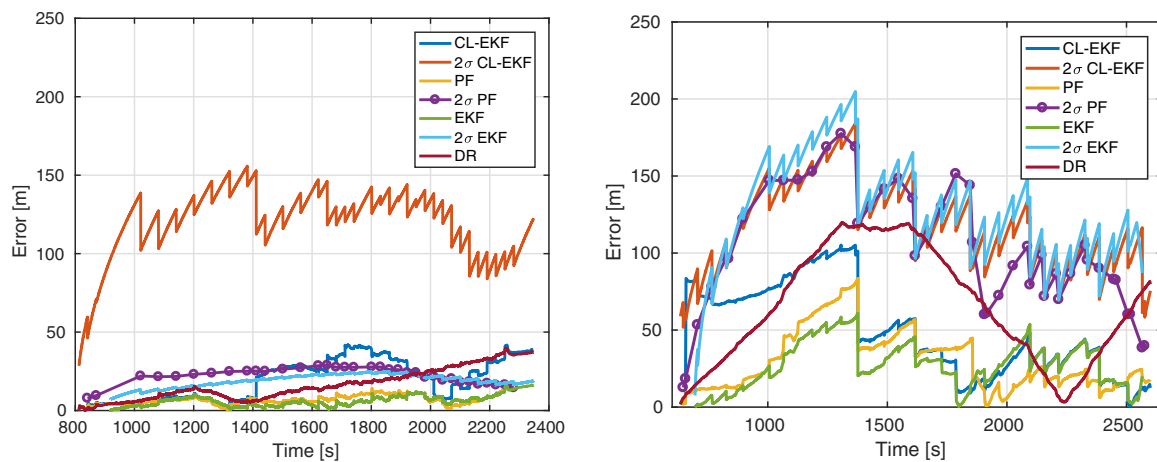


**FIGURE 11** Errors and  $2\sigma$  error bounds of Iver-106 (Left) and Iver-136 (Right) during the October 25, 2016 field trials in Ashumet Pond, MA. Here the Iver-106 CL-EKF solution uses DVL measurements while the Iver-136 CL-EKF uses a model velocity based dead-reckoning estimate. Off-line renavigation of each vehicle with the PF shows a reduction in error in Iver-106's case by reducing the  $\alpha_{DR}$  to 0.05 and in Iver-136's case by being less sensitive to the bad initial ranges

**TABLE 4** RMS errors for the closed-loop EKF (CL-EKFe), re-navigated EKF (EKFe), re-navigated PF (PFfe) and dead-reckoned (DRfe) solutions during the October 25 Ashumet Pond field trials for vehicle's Iver-106 and Iver-136 which use as their measurement update either a Doppler velocity log (DVL) or model velocity based dead-reckoning (M-DR)

Date	Vehicle	Measurement	CL-EKFe	EKFe	PFfe	DRfe
Oct25	106	DVL	19.6 m	6.2 m	6.3 m	16.5 m
Oct25	136	M-DR	51.0 m	27.4 m	25.8 m	67.5 m

Iver-136 was clearly underway. The R/V *Aurelia* was then launched, piloted out to deeper water and the topside transducer deployed. During this sequence, Iver-136 received ranges with bad beacon location estimates due to the navigation solution on the topside and Iver-106 not being initialized but the acoustic driver still transmitting on those platforms. This improper initialization sequence would typically be mitigated by the use of the GPS measurements while at the surface, however, in this instance, the GPS was used for initialization only. These bad beacon location estimates had the effect of biasing Iver-

136's closed-loop EKF estimate at the start of its mission as illustrated in Figure 10. In spite of this initial bias the closed-loop EKF solution managed to converge within 50 m of the GPS track after around 1500 s.

Iver-136's data was re-navigated with the EKF in post-processing to examine the effects of removing the two bad initial ranges. By removing these ranges the EKF solution remains much closer to the GPS measurements throughout. Additionally, the re-navigated EKF converges to the closed-loop solution after approximately 1800 s. The PF was also run in post-processing but allowed to take as inputs the two bad initial ranges. Here, the PF solution outperforms the EKF, converging faster and being more robust to outliers. Specifically, if the initial bad ranges are denied from the EKF solution in post-processing the error decreases to 27 m RMS from 51 m RMS and matches closed-loop solution after it has corrected for the initial bias. The PF solution in post-processing was found to be robust to the bad ranges, only deviating slightly and resulting in an error of 26 m RMS. These errors are contrasted with the dead reckoned error of 68 m RMS over a traversed distance of around 1600 m.

During Iver-106's mission the vehicle's DR error was significantly smaller relative to Iver-136's due to the use of the DVL measurements in the navigation solution. During the closed-loop EKF trials the  $\mathbf{Q}$  and  $\mathbf{R}$  values were kept the same as those used previously in Section 4.1 with the exception of the  $\sigma_{rng}$  which was set to 10 m. For this reason the performance of the Iver-106's closed-loop EKF with the DVL was similar to the performance of Iver-136's EKF, neglecting the bad initial ranges, which only used model velocities. However, a re-navigation of Iver-106's data with the EKF and PF where the  $\mathbf{Q}$  and  $\mathbf{R}$  values are reduced to account for the DVL measurements had the result of significantly reducing the RMS error. The values used for  $\mathbf{Q}$  and  $\mathbf{R}$  in Iver-106's re-navigated EKF are

$$\sigma_{vel} = 0.05 \text{ (m/s)} \quad (39)$$

$$\mathbf{Q} = \mathbf{I} * 0.01 \quad (40)$$

and in the re-navigated PF the  $\sigma_{DR}$  was reduced to 0.05:

$$\alpha_{DR} = 0.05. \quad (41)$$

Specifically, the closed-loop EKF solution had an error of around 20 m RMS on the DVL aided vehicle, Iver-106, compared with 17 m the dead-reckoning error, respectively. With the adjusted values used in post-processing the RMS error for the EKF and PF when the DVL is used decreased down to 6 m RMS. These errors are contrasted with a dead-reckoning error of 17 m RMS over a traversed distance of around 1600 m.

## 5 | CONCLUSIONS

To compute the one way travel time (OWTT) navigation updates two methods are presented, a tightly coupled extended Kalman filter (EKF) and a loosely coupled particle filter (PF). In the EKF solution, global positioning system (GPS), Doppler velocity log (DVL), model velocity and range measurements are fused into the EKF's estimates as available. During the range measurement update the EKF's state and covariance matrices are augmented to include the transmitting beacon's location and uncertainty. Conversely, the PF implementation runs on top of the EKF solution taking the place of the EKF during the range measurement update. During the range measurement update the PF uses the EKF's dead-reckoned solution to propagate the particles, computes a solution using the jittered bootstrapped PF algorithm and fuses the location update back into the EKF solution. In both the EKF and PF, the state estimates and range measurements may be used as an input to a bias estimator which computes a velocity and time synchronization bias. The bias estimator in this work is implemented as a loosely coupled Kalman filter whose outputs are used to augment the velocity estimates used in the dead-reckoning solution and the time of flight used in the range measurement.

These methods were developed using data gathered during field trials with two Iver-2 Autonomous Underwater Vehicles (AUVs) and a topside transducer dangled from the R/V *Shana Rae* in Monterey Bay,

CA on September 1 and 2, 2016. These trials were used to evaluate the short term and long term effectiveness of the EKF and PF, the utility of the bias estimator and the use of a topside only or all to all acoustic topology. In the short runs between GPS updates the PF was found to improve on the dead-reckoning solution whereas the EKF did not. When the GPS was used only for initialization, both the EKF and the PF improve on the dead-reckoning performance significantly with the PF slightly outperforming the EKF in most cases. If the bias estimator is not used or when only the topside beacon is used, the EKF and PF perform worse than when the bias estimator is used and all beacons are used.

The EKF solution without the bias estimator was then used in closed-loop trials on October 25, 2016 in Ashumet Pond, MA. In these trials two of the Iver-2 AUVs were used in addition to the topside installed on small rigid hull inflatable boat. One of the AUVs was allowed to use the DVL as input to the EKF whereas the other was not, providing a direct comparison between the closed-loop multi-vehicle OWTT navigation with a DVL and a model velocity dead-reckoning solution. In this case both vehicles maintained convergence with errors of 20 m RMS and 51 m RMS respectively despite the bad initial ranges received by the model velocity aided vehicle. In post-processing the DVL aided vehicle was able to have its error reduced to 6 m RMS in both the EKF and PF by adjusting the process noise values account for the DVL. Further, by removing the bad initial ranges from the EKF solution in post-processing it was found to converge to the closed-loop solution with an error of 27 m RMS. The PF solution was found to be robust to the bad initial ranges in post-processing with an error of 26 m RMS.

This work includes the first presentation of closed-loop one-way-travel-time navigation of a group of autonomous underwater vehicles aided by a topside beacon and extends prior contributions by using low-grade odometry on the AUVs for the navigation update through development of both an EKF solution and a PF solution. These estimators include a bias estimator which compensates both for persistent velocity errors due to water currents and modeling errors and for timing errors due to slowly drifting reference clocks. Further, the impact of the degraded navigation solution is quantified through a direct comparison between a DVL aided and model velocity based dead-reckoning navigation methods. These methods were developed through extensive open ocean field trials and validated in closed-loop in a local lake. Together, these contributions provide a demonstration of OWTT navigation methods suitable to vehicles equipped only with a low-grade odometry solution, acoustic modem and precision clock reference enabling low power and low cost navigation of groups of AUVs.

The limited requirements of these methods make it directly applicable to a diverse set of underwater navigation problems. Most directly, the emerging class of micro-AUVs will directly benefit from the low cost requirements of the needed hardware enabling further democratization of the use of AUVs. Further, this method is applicable to navigational aiding of long duration platforms such as autonomous underwater gliders and long range AUVs due its low energy requirements. It also provides a natural path for scaling the navigational accuracy of vehicles which have DVLs and only turn them on when high-accuracy navigation is needed. This work also provides a bounded navigational aid for AUVs

operating under ice, in the mid-water column and during their descent in deep water where DVLs are often out of range of the bottom. Additionally, if one or more AUVs is used as the topside beacon the research vessel is no longer needed enabling it to perform other tasks in the area or, in the case of long duration platforms, a completely ship-less survey.

## ACKNOWLEDGMENTS

This work was supported in part through funding from the Weston Howland Jr. Postdoctoral Scholar Award (BCC), the U.S. Navy's Civilian Institution program via the MIT/WHOI Joint Program (JHK), W. M. Keck Institute for Space Studies, and the Woods Hole Oceanographic Institution. The authors would like to thank Dr. Ben Hodges, who provided two of the AUVs used in these experiments, Dr. David Fratantoni, who assisted with the field experiments, Dr. Richard Camilli, who lent the boat used as the surface beacon in the Ashumet Pond field experiments, and Dr. Sarah Webster, who provided valuable insight and feedback. Captain Jim Christmann of the R/V Shana Rae ably supported our California field work.

## ORCID

Brian Claus  <http://orcid.org/0000-0003-2335-6053>

## REFERENCES

- Milne PH. *Underwater Acoustic Positioning Systems*. Houston, TX: Gulf Publishing; 1983.
- Parthiot FP, Denis J-F. A better way to navigate on deep sea floors. Paper presented at: OCEANS'93. Engineering in Harmony with Ocean. Proceedings; October 18–21, 1993; Piscataway, NY: IEEE.
- Hegrens Å, Gade K, Hagen OK, Hagen PE. Underwater transponder positioning and navigation of autonomous underwater vehicles. In: *OCEANS 2009*. Bixoli, MS. Piscataway, NY: MTS/IEEE. 2009:1–7.
- Kinsey JC, Eustice RM, Whitcomb LL. A survey of underwater vehicle navigation: Recent advances and new challenges. In: *IFAC Conference of Manoeuvring and Control of Marine Craft 2006*. Lisbon, Portugal. vol. 88. 2006.
- Paull L, Saeedi S, Seto M, Li H. AUV navigation and localization: A review. *IEEE J Oceanic Eng*. 2014;39(1):131–149.
- German C, Jakuba M, Kinsey J, et al. A long term vision for long-range ship-free deep ocean operations: Persistent presence through coordination of autonomous surface vehicles and autonomous underwater vehicles. In: *2012 IEEE/OES Autonomous Underwater Vehicles*. Southampton, UK. Piscataway, NY: IEEE; 2012:1–7.
- Kinsey J, Jakuba M, German C. A long term vision for long-range ship-free deep ocean operations: persistent presence through coordination of autonomous surface vehicles and autonomous underwater vehicles. In: *Workshop on Marine Robotics and Applications. Looking into the Crystal Ball: 20 years hence in Marine Robotics*, Canary Islands, Spain: Invited; 2013.
- Viquez OA, Fischell EM, Rypkema NR, Schmidt H. Design of a general autonomy payload for low-cost AUV. In: *2016 IEEE/OES Autonomous Underwater Vehicles (AUV)*. Tokyo, Japan. Piscataway, NY: IEEE/OES; 2016:151–155.
- Crowell J. Small AUV for hydrographic applications. In: *Proceedings of IEEE Oceans 2006*. Boston, MA. Piscataway, NY: IEEE; 2006:1–6.
- Rudnick DL, Davis RE, Eriksen CC, Fratantoni DM, Perry MJ. Underwater gliders for ocean research. *Mar Technol Soc J*. 2004;38(2):73–84.
- Hobson BW, Bellingham JG, Kieft B, McEwen R, Godin M, Zhang Y. Tethys-class long range AUVs-extending the endurance of propeller-driven cruising AUVs from days to weeks. In: *2012 IEEE/OES Autonomous Underwater Vehicles (AUV)*. Southampton, UK. Piscataway, NY: IEEE; 2012:1–8.
- Medagoda L, Kinsey JC, Eilders M. Autonomous underwater vehicle localization in a spatiotemporally varying water current field. In: *2015 IEEE International Conference on Robotics and Automation (ICRA)*. Seattle, WA. Piscataway, NY: IEEE; 2015:565–572.
- McFarland CJ, Jakuba MV, Suman S, Kinsey JC, Whitcomb LL. Toward ice-relative navigation of underwater robotic vehicles under moving sea ice: Experimental evaluation in the arctic sea. In: *2015 IEEE International Conference on Robotics and Automation (ICRA)*. Seattle, WA. Piscataway, NY: IEEE; 2015:1527–1534.
- Gardner AT, Collins JA. Advancements in high-performance timing for long term underwater experiments: A comparison of chip scale atomic clocks to traditional microprocessor-compensated crystal oscillators. In: *Oceans 2012*. Hampton Roads, VA. Piscataway, NY: IEEE; 2012:1–8.
- Eustice RM, Singh H, Whitcomb LL. Synchronous-clock, one-way-travel-time acoustic navigation for underwater vehicles. *J Field Robotics*. 2011;28(1):121–136.
- Gardner AT, Collins JA. A second look at chip scale atomic clocks for long term precision timing. In: *OCEANS 2016 MTS/IEEE Monterey*. Monterey, CA. Piscataway, NY: IEEE; 2016:1–9.
- Gadre AS, Stilwell DJ. A complete solution to underwater navigation in the presence of unknown currents based on range measurements from a single location. In: *2005 IEEE/RSJ International Conference on Intelligent Robots and Systems*. Edmonton, Canada. Piscataway, NY: IEEE; 2005:1420–1425.
- Song TL. Observability of target tracking with range-only measurements. *IEEE J Oceanic Eng*. 1999;24(3):383–387.
- Walls JM, Chaves SM, Galceran E, Eustice RM. Belief space planning for underwater cooperative localization. In: *2015 IEEE/RSJ International Conference on Intelligent Robots and Systems (IROS)*. Hamburg, Germany. Piscataway, NY: IEEE; 2015:2264–2271.
- Roumeliotis SI, Bekey GA. Distributed multirobot localization. *IEEE T Robot Autom*. 2002;18(5):781–795.
- Bahr A, Leonard JJ, Fallon MF. Cooperative localization for autonomous underwater vehicles. *Int J Robot Res*. 2009;28(6):714–728.
- Paull L, Seto M, Leonard JJ. Decentralized cooperative trajectory estimation for autonomous underwater vehicles. In: *2014 IEEE/RSJ International Conference on Intelligent Robots and Systems*. Chicago, IL. Piscataway, NY: IEEE; 2014:184–191.
- Bahr A, Walter MR, Leonard JJ. Consistent cooperative localization. In: *2009 IEEE International Conference on Robotics and Automation (ICRA)*. Kobe, Japan. Piscataway, NY: IEEE; 2009:3415–3422.
- Walls JM, Cunningham AG, Eustice RM. Cooperative localization by factor composition over a faulty low-bandwidth communication channel. In: *2015 IEEE International Conference on Robotics and Automation (ICRA)*. Seattle, WA. Piscataway, NY: IEEE; 2015:401–408.
- Maczka DK, Gadre AS, Stilwell DJ. Implementation of a cooperative navigation algorithm on a platoon of autonomous underwater vehicles. In: *OCEANS 2007*. Piscataway, NY: IEEE; 2007:1–6.
- Webster SE. *Decentralized single-beacon acoustic navigation: Combined communication and navigation for underwater vehicles*. [Dissertation]. Technical report, Baltimore, MD: Johns Hopkins University; 2010.



27. Tan YT, Chitre M, Hover FS. Cooperative bathymetry-based localization using low-cost autonomous underwater vehicles. *Auton Robot*. 2016;40(7):1187–1205.
28. Webster SE, Freitag LE, Lee CM, Gobat JI. Towards real-time under-ice acoustic navigation at mesoscale ranges. In: *2015 IEEE International Conference on Robotics and Automation (ICRA)*. Seattle, WA. Piscataway, NY: IEEE; 2015:537–544.
29. Thompson A, Kinsey JC, Coleman M, Castano B, Rebecca scl. *Satellites to the seafloor: Autonomous science to forge a breakthrough in quantifying the global ocean carbon budget*. Technical report, Pasadena, CA: Keck Institute for Space Studies, California Institute of Technology; 2015. <http://www.kiss.caltech.edu/study/seafloor>.
30. Bar-Shalom Y, Li XR, Kirubarajan T. *Estimation with Applications to Tracking and Navigation: Theory Algorithms and Software*. Hoboken, NJ: John Wiley & Sons; 2001.
31. Gadre AS, Stilwell DJ. Toward underwater navigation based on range measurements from a single location. In: *2004 IEEE International Conference on Robotics and Automation (ICRA)*. vol 5. New Orleans, LA. Piscataway, NY: IEEE; 2004:4472–4477.
32. Grewal MS, Andrews AP. *Kalman filtering: Theory and Practice Using MATLAB*. 2nd ed. Hoboken, NJ: John Wiley & Sons; 2001.
33. Bucy RS, Joseph PD. *Filtering for Stochastic Processes with Applications to Guidance*. 2nd ed. New York: Chelsea Publishers; 1987.
34. Walls JM, Eustice RM. Experimental comparison of synchronous-clock cooperative acoustic navigation algorithms. In: *OCEANS'11 MTS/IEEE KONA*. Waikoloa, HI. Piscataway, NY: IEEE; 2011:1–7.
35. Webster SE, Eustice RM, Singh H, Whitcomb LL. Advances in single-beacon one-way-travel-time acoustic navigation for underwater vehicles. *Int J Robot Res*. 2012;31(8):935–950.
36. Kitagawa G. Monte carlo filter and smoother for non-gaussian nonlinear state space models. *J Comput Graph Stat*. 1996;5(1):1–25.
37. Teixeira FJCM. *Terrain-Aided Navigation and Geophysical Navigation of Autonomous Underwater Vehicles*. PhD thesis, Universidade Tecnica De Lisboa Instituto Superior Tecnico; 2007.
38. Gallimore E, Partan J, Vaughn I, Singh S, Shusta J, Freitag L. The WHOI micromodem-2: A scalable system for acoustic communications and networking. In: *OCEANS 2010*. Seattle, WA. Piscataway, NY: IEEE; 2010:1–7.
39. Huang AS, Olson E, Moore DC. LCM: Lightweight communications and marshalling. In: *2010 IEEE/RSJ International Conference on Intelligent Robots and Systems (IROS)*. Taipei, Taiwan. Piscataway, NY: IEEE; 2010:4057–4062.
40. Eustice RM, Whitcomb LL, Singh H, Grund M. Recent advances in synchronous-clock one-way-travel-time acoustic navigation. In: *OCEANS 2006*. Boston, MA. Piscataway, NY: IEEE; 2006:1–6.
41. Eustice RM, Whitcomb LL, Singh H, Grund M. Experimental results in synchronous-clock one-way-travel-time acoustic navigation for autonomous underwater vehicles. In: *2007 IEEE International Conference on Robotics and Automation*. Roma, Italy. Piscataway, NY: IEEE; 2007:4257–4264.

**How to cite this article:** Claus B, Keppler JH IV, Suman S, Kinsey JC. Closed-loop one-way-travel-time navigation using low-grade odometry for autonomous underwater vehicles. *J Field Robotics*. 2017;00:1–14. <https://doi.org/10.1002/rob.21746>